Biomedical Optics EXPRESS

Artificially-induced organelles are optimal targets for optical trapping experiments in living cells

C. López-Quesada,[1] A.-S. Fontaine,[1] A. Farré,[1] M. Joseph,[2] J. Selva,[3,4] G. Egea,[3,4] M. D. Ludevid,[2] E. Martín-Badosa,[1,4] and M. Montes-Usategui[1,4,*]

[1]*Optical Trapping Lab – Grup de Biofotònica, Departament de Física Aplicada i Òptica, Universitat de Barcelona, Martí i Franquès 1, 08028 Barcelona, Spain*
[2]*Department of Molecular Genetics, Center for Research in Agricultural Genomics (CRAG) CSIC-IRTA-UAB-UB, Campus Universitat Autònoma de Barcelona, Bellaterra (Cerdanyola del Vallès), 08193 Barcelona, Spain*
[3]*Departament de Biologia Cel·lular, Immunologia i Neurociències, Facultat de Medicina, Universitat de Barcelona and Institut d'Investigacions Biomèdiques August Pi i Sunyer (IDIBAPS), 08036 Barcelona, Spain*
[4]*Institut de Nanociència i Nanotecnologia (IN2UB), U. de Barcelona, Martí i Franquès 1, 08028 Barcelona, Spain*
[*]*mario_montes@ub.edu*

Abstract: Optical trapping supplies information on the structural, kinetic or rheological properties of inner constituents of the cell. However, the application of significant forces to intracellular objects is notoriously difficult due to a combination of factors, such as the small difference between the refractive indices of the target structures and the cytoplasm. Here we discuss the possibility of artificially inducing the formation of spherical organelles in the endoplasmic reticulum, which would contain densely packed engineered proteins, to be used as optimized targets for optical trapping experiments. The high index of refraction and large size of our organelles provide a firm grip for optical trapping and thereby allow us to exert large forces easily within safe irradiation limits. This has clear advantages over alternative probes, such as subcellular organelles or internalized synthetic beads.

OCIS codes: (140.7010) Laser trapping; (170.4520) Optical confinement and manipulation; (350.4855) Optical tweezers or optical manipulation; (170.1530) Cell analysis.

References and links

1. B. D. Hoffman and J. C. Crocker, "Cell mechanics: dissecting the physical responses of cells to force," Annu. Rev. Biomed. Eng. **11**(1), 259–288 (2009).
2. B. D. Hoffman, C. Grashoff, and M. A. Schwartz, "Dynamic molecular processes mediate cellular mechanotransduction," Nature **475**(7356), 316–323 (2011).
3. Y. F. Dufrêne, E. Evans, A. Engel, J. Helenius, H. E. Gaub, and D. J. Müller, "Five challenges to bringing single-molecule force spectroscopy into living cells," Nat. Methods **8**(2), 123–127 (2011).
4. M. T. Wei, A. Zaorski, H. C. Yalcin, J. Wang, S. N. Ghadiali, A. Chiou, and H. D. Ou-Yang, "A comparative study of living cell micromechanical properties by oscillatory optical tweezers," Opt. Express **16**(12), 8594–8603 (2008).
5. T. Ketelaar, H. S. van der Honing, and A. M. C. Emons, "Probing cytoplasmic organization and the actin cytoskeleton of plant cells with optical tweezers," Biochem. Soc. Trans. **38**(3), 823–828 (2010).
6. I. A. Sparkes, T. Ketelaar, N. C. A. de Ruijter, and C. Hawes, "Grab a Golgi: laser trapping of Golgi bodies reveals *in vivo* interactions with the endoplasmic reticulum," Traffic **10**(5), 567–571 (2009).
7. C. Hawes, A. Osterrieder, I. A. Sparkes, and T. Ketelaar, "Optical tweezers for the micromanipulation of plant cytoplasm and organelles," Curr. Opin. Plant Biol. **13**(6), 731–735 (2010).
8. M. X. Andersson, M. Goksör, and A. S. Sandelius, "Optical manipulation reveals strong attracting forces at membrane contact sites between endoplasmic reticulum and chloroplasts," J. Biol. Chem. **282**(2), 1170–1174 (2007).
9. K. Hayakawa, H. Tatsumi, and M. Sokabe, "Actin stress fibers transmit and focus force to activate mechanosensitive channels," J. Cell Sci. **121**(4), 496–503 (2008).

#209469 - $15.00 USD Received 4 Apr 2014; revised 24 May 2014; accepted 25 May 2014; published 30 May 2014

10. G. T. Shubeita, S. L. Tran, J. Xu, M. Vershinin, S. Cermelli, S. L. Cotton, M. A. Welte, and S. P. Gross, "Consequences of motor copy number on the intracellular transport of Kinesin-1-driven lipid droplets," Cell **135**, 1098–1107 (2008).
11. C. Leidel, R. A. Longoria, F. M. Gutierrez, and G. T. Shubeita, "Measuring molecular motor forces in vivo: implications for tug-of-war models of bidirectional transport," Biophys. J. **103**(3), 492–500 (2012).
12. J. Yoo, T. Kambara, K. Gonda, and H. Higuchi, "Intracellular imaging of targeted proteins labeled with quantum dots," Exp. Cell Res. **314**(19), 3563–3569 (2008).
13. R. Bar-Ziv, E. Moses, and P. Nelson, "Dynamic excitations in membranes induced by optical tweezers," Biophys. J. **75**(1), 294–320 (1998).
14. V. Bormuth, A. Jannasch, M. Ander, C. M. van Kats, A. van Blaaderen, J. Howard, and E. Schäffer, "Optical trapping of coated microspheres," Opt. Express **16**(18), 13831–13844 (2008).
15. A. Jannasch, A. F. Demirörs, P. D. J. van Oostrum, A. van Blaaderen, and E. Schäffer, "Nanonewton optical force trap employing anti-reflection coated, high-refractive-index titania microspheres," Nat. Photonics **6**(7), 469–473 (2012).
16. V. Olivier, J.-L. Duval, M. Hindié, P. Pouletaut, and M.-D. Nagel, "Comparative particle-induced cytotoxicity toward macrophages and fibroblasts," Cell Biol. Toxicol. **19**(3), 145–159 (2003).
17. L. M. Costantini, R. M. Gilberti, and D. A. Knecht, "The phagocytosis and toxicity of amorphous silica," PLoS ONE **6**(2), e14647 (2011).
18. S. P. Gross, "Come together: group behavior of dynein motors," Dev. Cell **24**(2), 117–118 (2013).
19. L. B. Oddershede, "Force probing of individual molecules inside the living cell is now a reality," Nat. Chem. Biol. **8**(11), 879–886 (2012).
20. R. Drezek, A. Dunn, and R. Richards-Kortum, "Light scattering from cells: finite-difference time-domain simulations and goniometric measurements," Appl. Opt. **38**(16), 3651–3661 (1999).
21. S. P. Gross, "Application of optical traps in vivo," Methods Enzymol. **361**, 162–174 (2003).
22. M. A. Welte, S. P. Gross, M. Postner, S. M. Block, and E. F. Wieschaus, "Developmental regulation of vesicle transport in Drosophila embryos: forces and kinetics," Cell **92**(4), 547–557 (1998).
23. C. Veigel and C. F. Schmidt, "Moving into the cell: single-molecule studies of molecular motors in complex environments," Nat. Rev. Mol. Cell Biol. **12**(3), 163–176 (2011).
24. A. T. Lada, M. C. Willingham, and R. W. St Clair, "Triglyceride depletion in THP-1 cells alters cholesteryl ester physical state and cholesterol efflux," J. Lipid Res. **43**(4), 618–628 (2002).
25. X. Nan, J. X. Cheng, and X. S. Xie, "Vibrational imaging of lipid droplets in live fibroblast cells with coherent anti-Stokes Raman scattering microscopy," J. Lipid Res. **44**(11), 2202–2208 (2003).
26. D. Débarre, W. Supatto, A. M. Pena, A. Fabre, T. Tordjmann, L. Combettes, M. C. Schanne-Klein, and E. Beaurepaire, "Imaging lipid bodies in cells and tissues using third-harmonic generation microscopy," Nat. Methods **3**(1), 47–53 (2006).
27. T. Watanabe, A. Thayil, A. Jesacher, K. Grieve, D. Debarre, T. Wilson, M. Booth, and S. Srinivas, "Characterisation of the dynamic behaviour of lipid droplets in the early mouse embryo using adaptive harmonic generation microscopy," BMC Cell Biol. **11**(1), 38 (2010).
28. G. Galili, "ER-derived compartments are formed by highly regulated processes and have special functions in plants," Plant Physiol. **136**(3), 3411–3413 (2004).
29. M. I. Geli, M. Torrent, and D. Ludevid, "Two structural domains mediate two sequential events in γ-zein targeting: protein endoplasmic reticulum retention and protein body formation," Plant Cell **6**(12), 1911–1922 (1994).
30. M. Torrent, B. Llompart, S. Lasserre-Ramassamy, I. Llop-Tous, M. Bastida, P. Marzabal, A. Westerholm-Parvinen, M. Saloheimo, P. B. Heifetz, and M. D. Ludevid, "Eukaryotic protein production in designed storage organelles," BMC Biol. **7**(1), 5 (2009).
31. I. Llop-Tous, M. Ortiz, M. Torrent, and M. D. Ludevid, "The expression of a xylanase targeted to ER-protein bodies provides a simple strategy to produce active insoluble enzyme polymers in tobacco plants," PLoS ONE **6**(4), e19474 (2011).
32. M. Torrent, I. Llop-Tous, and M. D. Ludevid, "Protein body induction: a new tool to produce and recover recombinant proteins in plants," Methods Mol. Biol. **483**, 193–208 (2009).
33. I. Llop-Tous, S. Madurga, E. Giralt, P. Marzabal, M. Torrent, and M. D. Ludevid, "Relevant elements of a maize gamma-zein domain involved in protein body biogenesis," J. Biol. Chem. **285**(46), 35633–35644 (2010).
34. E. M. Herman and B. A. Larkins, "Protein storage bodies and vacuoles," Plant Cell **11**(4), 601–614 (1999).
35. R. M. Simmons, J. T. Finer, S. Chu, and J. A. Spudich, "Quantitative measurements of force and displacement using an optical trap," Biophys. J. **70**(4), 1813–1822 (1996).
36. A. Rohrbach, "Stiffness of optical traps: quantitative agreement between experiment and electromagnetic theory," Phys. Rev. Lett. **95**(16), 168102 (2005).
37. K. C. Neuman, E. H. Chadd, G. F. Liou, K. Bergman, and S. M. Block, "Characterization of photodamage to Escherichia coli in optical traps," Biophys. J. **77**(5), 2856–2863 (1999).
38. T. A. Nieminen, V. L. Y. Loke, A. B. Stilgoe, G. Knöner, A. M. Brańczyk, N. R. Heckenberg, and H. Rubinsztein-Dunlop, "Optical tweezers computational toolbox," J. Opt. A, Pure Appl. Opt. **9**(8), S196–S203 (2007).
39. G. Knöner, S. Parkin, T. A. Nieminen, N. R. Heckenberg, and H. Rubinsztein-Dunlop, "Measurement of the index of refraction of single microparticles," Phys. Rev. Lett. **97**(15), 157402 (2006).

#209469 - $15.00 USD Received 4 Apr 2014; revised 24 May 2014; accepted 25 May 2014; published 30 May 2014

40. A. Ashkin, “Forces of a single-beam gradient laser trap on a dielectric sphere in the ray optics regime,” Biophys. J. **61**(2), 569–582 (1992).
41. R. Barer and S. Joseph, “Refractometry of living cells, part I. Basic principles,” Q. J. Microsc. Sci. **95**, 399–423 (1954).
42. H. Zhao, P. H. Brown, and P. Schuck, “On the distribution of protein refractive index increments,” Biophys. J. **100**(9), 2309–2317 (2011).
43. J. Vörös, “The Density and Refractive Index of Adsorbing Protein Layers,” Biophys. J. **87**(1), 553–561 (2004).
44. H. Fischer, I. Polikarpov, and A. F. Craievich, “Average protein density is a molecular-weight-dependent function,” Protein Sci. **13**(10), 2825–2828 (2004).
45. M. Joseph, M. D. Ludevid, M. Torrent, V. Rofidal, M. Tauzin, M. Rossignol, and J.-B. Peltier, “Proteomic characterisation of endoplasmic reticulum-derived protein bodies in tobacco leaves,” BMC Plant Biol. **12**(1), 36 (2012).
46. R. Barer, “Refractometry and interferometry of living cells,” J. Opt. Soc. Am. **47**(6), 545–556 (1957).
47. J. Guck, S. Schinkinger, B. Lincoln, F. Wottawah, S. Ebert, M. Romeyke, D. Lenz, H. M. Erickson, R. Ananthakrishnan, D. Mitchell, J. Käs, S. Ulvick, and C. Bilby, “Optical deformability as an inherent cell marker for testing malignant transformation and metastatic competence,” Biophys. J. **88**(5), 3689–3698 (2005).
48. J. Mas, A. C. Richardson, S. N. S. Reihani, L. B. Oddershede, and K. Berg-Sørensen, “Quantitative determination of optical trapping strength and viscoelastic moduli inside living cells,” Phys. Biol. **10**(4), 046006 (2013).
49. C. L. Curl, C. J. Bellair, T. Harris, B. E. Allman, P. J. Harris, A. G. Stewart, A. Roberts, K. A. Nugent, and L. M. D. Delbridge, “Refractive index measurement in viable cells using quantitative phase-amplitude microscopy and confocal microscopy,” Cytometry A **65A**(1), 88–92 (2005).
50. K. Visscher, S. P. Gross, and S. M. Block, “Construction of multiple-beam optical traps with nanometer-resolution position sensing,” IEEE J. Sel. Top. Quantum Electron. **2**(4), 1066–1076 (1996).
51. K. Berg-Sørensen and H. Flyvbjerg, “Power spectrum analysis for optical tweezers,” Rev. Sci. Instrum. **75**(3), 594–612 (2004).
52. A. Farré, F. Marsà, and M. Montes-Usategui, “Optimized back-focal-plane interferometry directly measures forces of optically trapped particles,” Opt. Express **20**(11), 12270–12291 (2012).
53. J. Beuthan, O. Minet, J. Helfmann, M. Herrig, and G. Müller, “The spatial variation of the refractive index in biological cells,” Phys. Med. Biol. **41**(3), 369–382 (1996).
54. G. F. Zhang and L. A. Staehelin, “Functional compartmentation of the Golgi apparatus of plant cells : immunocytochemical analysis of high-pressure frozen- and freeze-substituted sycamore maple suspension culture cells,” Plant Physiol. **99**(3), 1070–1083 (1992).
55. P. Boevink, K. Oparka, S. Santa Cruz, B. Martin, A. Betteridge, and C. Hawes, “Stacks on tracks: the plant Golgi apparatus traffics on an actin/ER network,” Plant J. **15**(3), 441–447 (1998).
56. S. Bayoudh, T. A. Nieminen, N. R. Heckenberg, and H. Rubinsztein-Dunlop, “Orientation of biological cells using plane-polarized Gaussian beam optical tweezers,” J. Mod. Opt. **50**(10), 1581–1590 (2003).
57. I. Derényi, F. Jülicher, and J. Prost, “Formation and interaction of membrane tubes,” Phys. Rev. Lett. **88**(23), 238101 (2002).
58. G. Koster, A. Cacciuto, I. Derényi, D. Frenkel, and M. Dogterom, “Force barriers for membrane tube formation,” Phys. Rev. Lett. **94**(6), 068101 (2005).
59. T. Shimmen and E. Yokota, “Cytoplasmic streaming in plants,” Curr. Opin. Cell Biol. **16**(1), 68–72 (2004).
60. I. A. Sparkes, L. Frigerio, N. Tolley, and C. Hawes, “The plant endoplasmic reticulum: a cell-wide web,” Biochem. J. **423**(2), 145–155 (2009).
61. A. Ashkin and J. M. Dziedzic, “Internal cell manipulation using infrared laser traps,” Proc. Natl. Acad. Sci. U.S.A. **86**(20), 7914–7918 (1989).
62. S. Yamada, D. Wirtz, and S. C. Kuo, “Mechanics of living cells measured by laser tracking microrheology,” Biophys. J. **78**(4), 1736–1747 (2000).
63. T. Lobovkina, P. G. Dommersnes, S. Tiourine, J.-F. Joanny, and O. Orwar, “Shape optimization in lipid nanotube networks,” Eur Phys J E Soft Matter **26**(3), 295–300 (2008).
64. E. Yokota, H. Ueda, K. Hashimoto, H. Orii, T. Shimada, I. Hara-Nishimura, and T. Shimmen, “Myosin XI-dependent formation of tubular structures from endoplasmic reticulum isolated from tobacco cultured BY-2 cells,” Plant Physiol. **156**(1), 129–143 (2011).
65. I. Sparkes, J. Runions, C. Hawes, and L. Griffing, “Movement and remodeling of the endoplasmic reticulum in nondividing cells of tobacco leaves,” Plant Cell **21**(12), 3937–3949 (2009).
66. E. Martín-Badosa, M. Montes-Usategui, A. Carnicer, J. Andilla, E. Pleguezuelos, and I. Juvells, “Design strategies for optimizing holographic optical tweezers set-ups,” J. Opt. A, Pure Appl. Opt. **9**(8), S267–S277 (2007).
67. E. Pleguezuelos, A. Carnicer, J. Andilla, E. Martín-Badosa, and M. Montes-Usategui, “HoloTrap: interactive hologram design for multiple dynamic optical trapping,” Comput. Phys. Commun. **176**(11-12), 701–709 (2007).
68. E. Goytia, L. Fernández-Calvino, B. Martínez-García, D. López-Abella, and J. J. López-Moya, “Production of plum pox virus HC-Pro functionally active for aphid transmission in a transient-expression system,” J. Gen. Virol. **87**(11), 3413–3423 (2006).
69. O. Voinnet, S. Rivas, P. Mestre, and D. Baulcombe, “An enhanced transient expression system in plants based on suppression of gene silencing by the p19 protein of tomato bushy stunt virus,” Plant J. **33**(5), 949–956 (2003).

#209469 - $15.00 USD Received 4 Apr 2014; revised 24 May 2014; accepted 25 May 2014; published 30 May 2014

1. Introduction

The capacity to generate, sustain and transduce forces across different length scales is crucial in many cellular mechanisms, including DNA transcription and replication, membrane trafficking, cytoskeletal reorganization, cell motility and mechanosensing [1–3]. Force spectroscopy techniques allow experiments both at the molecular level and on bulk cell structures. Building on tremendous recent progress *in vitro*, these techniques are increasingly being applied *in vivo*, and potentially provide information on complex cellular and molecular processes that is ultimately limited by our capacity for analysis and interpretation [2].

Among force spectroscopy techniques, optical trapping stands out for its capacity to operate at a distance but affect only a small spatial region. Lateral displacement of a highly focused laser beam allows relocation of dielectric particles due to radiation pressure, which enables precise, three-dimensional positioning of micrometric and nanometric structures. Integrated optical trapping and microscopy may thus be used as a powerful tool to link changes in physical aspects of intracellular organization with the action of specific proteins, across a key range of forces (0.1 to 100 pN).

Mechanical stress, for example, is an interesting phenomenon that can change not only cell morphology, but also the cell cycle, gene expression and protein production. This prompted measurement of the intracellular viscoelasticity of alveolar epithelial cells, in order to understand pulmonary physiology at the cellular and molecular levels [4]. Similarly, actin filament binding proteins and molecular motors play an important role in the organization of the cytoplasm in plant cells, and optical tweezers are the ideal tool to elucidate the physical properties that provide the cytoplasm with this organization [5]. Strikingly, forming protrusions with optical tweezers revealed that their genesis resides in a myosin-motor-based relocation of actin filaments, rather than a *de novo* synthesis of actin filaments [6, 7]. Other experiments demonstrate that there is physical contact between chloroplasts and the endoplasmic reticulum (ER), or the Golgi apparatus and ER membranes. The study of such membrane contact sites is crucial to gaining an understanding of intracellular transport in plant cells [6, 8].

In general, in all these examples, measuring physical parameters allowed us to discover and unravel new information not achievable in biochemical or molecular assays, and which has proved indispensable for our understanding of biological processes. However, despite these successful examples of applications, optical trapping is not well suited to intracellular experiments, partly because of the inadequacy of the intracellular probes available.

Traditionally, optical tweezers have been used in assays in which biological function is reconstituted from purified proteins and cell extracts *in vitro*. These *in vitro* systems allow individual subcellular components (single molecular motors or individual cytoskeletal filaments, for example) to be probed without interference from other living processes. They thereby enable optical trapping to be carried out in a controlled environment, where force measurements can be performed accurately. Unfortunately, this approach can also miss important interactions with accessory proteins or regulatory factors, and provide data that differ from values observed *in vivo*, with important biological implications. For example, stall forces of both dynein and kinesin appear significantly different measured *in vivo* and *in vitro* [10, 11], or the motion of kinesin is noticeable different inside a cell from that observed in a single-molecule assay [12]. *In vivo* experiments are thus the yardstick against which *in vitro* information should ultimately be compared.

Although an optical trap can interact directly with the subcellular structures being studied (for example, lipid membranes [13]), it often does so indirectly by capturing a spherical handle to which the sample is attached. This ensures three-dimensional stable trapping, allows larger loads to be exerted and very particularly enables the calibration of the optical trap by applying known Stokes or Langevin forces. The handles commonly used *in vitro* are synthetic

#209469 - $15.00 USD Received 4 Apr 2014; revised 24 May 2014; accepted 25 May 2014; published 30 May 2014

microspheres whose size, structure and index of refraction can be chosen to fit the application [14, 15].

Unfortunately, the use of artificial microspheres is more difficult *in vivo*. Although microspheres can be spontaneously internalized by a cell or microinjected, the presence of microspheres inside cells can interfere with their biological functions [3, 16, 17]. For instance, the discrepancies between recent stall force measurements of kinesin and dynein may be due to distinctive behavior of the molecular motors when transporting endomembrane systems such as phagosomes [18]. Also, artificial microspheres tend to be relocated by the cell to storing sites and eventually become unavailable for optical manipulation [19].

The preferred approach is the manipulation of internal organelles, despite these typically having an index of refraction (n_o ~1.38-1.41) close to that of the cytoplasm (n_c ~1.36-1.375) [20] and thus only being adequate for the exertion of small forces. When the internal processes studied involve larger forces [21], specific structures with a high index of refraction such as lipid droplets (n_d ~1.48-1.53) are then the only option [22, 23]. Unfortunately, lipid droplets in turn present some drawbacks: they may be few or inappropriately small, or they may show cell-to-cell heterogeneities [24], which adds uncertainty to *in vivo* force calibrations based on purified vesicles from other cells. Finally, lipid droplets are difficult to identify *in vivo* unambiguously since most available dyes are efficiently effluxed by cells and only work after fixation [25–27].

Here we propose an alternative to overcome some of these difficulties by controllably inducing intracellular vesicles that unite useful aspects of both artificial and endogenous particles. A proline-rich N-terminal domain (Zera) derived from the maize storage protein γ-zein is by itself sufficient to induce large and spherical organelles called protein bodies (PBs). PBs are generated from the ER, both in transfected mammalian cells (Fig. 1(a)) and in genetically transformed plants (Fig. 1(b)). They appear to be excellent targets for optical trapping experiments inside living cells. Here, we present a characterization of their optical properties and provide examples of their application *in vivo*.

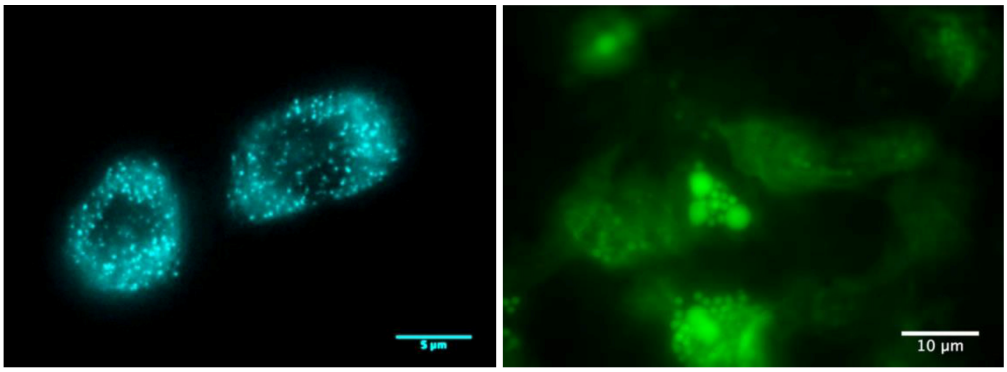

(a) (b)

Fig. 1. Fluorescent PBs induced in (a) Chinese Hamster Ovary (CHO) and (b) *Nicotiana benthamiana* (tobacco) cells.

2. Protein bodies are derived from the endoplasmic reticulum

The ER has the largest surface area of the organelles in eukaryotic cells and supports diverse cellular functions, including synthesis of proteins and lipids, maintenance of calcium homeostasis, and quality control of proteins. The ER forms a dynamic polygonal network composed of tubules, sheets, and three-way junctions. In addition to these highly conserved structures, some organisms develop characteristic ER-derived structures. For example, plant seeds are able to naturally store large reservoirs of storage proteins in specialized ER-derived compartments called PBs [28]. γ-Zein, is a storage protein that accumulates in PBs in maize

#209469 - $15.00 USD Received 4 Apr 2014; revised 24 May 2014; accepted 25 May 2014; published 30 May 2014

seeds. The proline-rich N-terminal sequence of γ-zein that comprises the first 93 amino acids (namely Zera) was shown to induce its stable accumulation in ER-derived PB-like structures in non-seed plant tissues [29]. To exploit the natural mechanism of protein accumulation which occurs in seed, an approach has been reported that produces a variety of recombinant proteins accumulated in the PBs of plant and animal cells [30, 31]. The approach relies on fusion proteins that contain the γ-zein signal peptide, the Zera sequence and a protein of interest fused to the C-terminus of the proline-rich region. Chimeric genes expressed in tobacco plants or animal cells accumulate fusion proteins encapsulated in ER-derived PBs. Zera-fusion proteins remain stable within membrane-bound PBs. These newly formed PB-like structures have two main features: a) they are dense organelles which can easily be recovered by density selection techniques [32] and b) their presence inside cells does not seem to disrupt the normal growth or development of plants or animal cell cultures.

The mechanism by which Zera forms these novel organelles has not yet been fully characterized. However, recent studies demonstrate relevant traits of the Zera sequence involved in *de novo* PB formation [33]. The presence of cysteine residues in the Zera sequence participates in the inter-disulfide bonds between Zera sequences, and its amphipathic feature determines the efficiency of Zera–Zera self-assembly by hydrophobic interactions. Although expressed in the leaves of plants, these novel PBs appeared similar in size and morphology to PBs that occur naturally in plant seeds [34].

The dense core resulting from the aggregation, accumulation and encapsulation of proteins makes the induced PBs highly refractive targets and easily trapped with optical tweezers. Furthermore, *ad hoc* fusions encoding specific proteins could enable certain control over the index of refraction of the resulting organelles, since the refractive index of proteins is known to depend on their particular sequence of amino acids (see Section 3.2). Also, Zera expression can be genetically modified to be fusioned with fluorescent proteins such as CFP (Fig. 1(a)) or GFP (Fig. 1(b)).

3. Trapping forces

Two different parameters are commonly used to determine the efficiency of an optical trap: the escape force and the stiffness, κ. Both are dependent on a number of properties of the trapping beam such as the numerical aperture or power, but are also notably affected by the size and refractive index of the sample. The size and refractive index of PBs are highly suitable for intracellular trapping experiments.

3.1 Size

Size is the single most important factor affecting the stiffness of an optical trap. The stiffness increases with the third power of diameter (d) for small Rayleigh particles, but the two magnitudes are inversely proportional for large Mie samples. In the intermediate region (described well by the generalized Lorenz-Mie theory), a sample size that maximizes trap stiffness can thus be found at around $d \sim \lambda/n_c$ [35, 36], where λ is the wavelength of the trapping laser in vacuum and n_c the refractive index of the surrounding medium (cytoplasm). For the most common trapping wavelength of λ = 1064 nm, we have d ~0.8 μm. Lipid droplets are smaller than this optimal value ($d_{typical}$ ~0.5 μm [11, 22]).

In contrast, in transient transformations of tobacco leaves with Zera fused to a fluorescent protein, despite some internal variability, there is a progressive increase in PB size over time that correlates with the capacity of protein synthesis machinery of the cell. At 2 days post-transformation, the PB diameters range from 0.5 to 1 μm, whereas at 7 days post-transformation, many PBs are larger than 1.5 μm (up to ~3 μm) [33]. PBs with sizes that optimize the stiffness can thus easily be found, which allow for forces within the linear region of the trap of several tens of pN (see Fig. 2 and Table 1). The growing of PBs could be arrested at this point by treatments with protein synthesis inhibitors such as cycloheximide. However, the cells will always contain a population of particles with different sizes as ER-

#209469 - $15.00 USD Received 4 Apr 2014; revised 24 May 2014; accepted 25 May 2014; published 30 May 2014

derived particles are produced along the ER in an asynchronous way. This would result in PB's size distributions centered around the target value but with a dispersion that increases with average size [33].

On the other hand, the maximum attainable force increases with increasing object diameter and eventually reaches a maximum for a diameter between 4 and 5 µm, beyond which force slowly decreases (Fig. 2). The large size of PBs a few days after the transformation allow us to approach this maximum force region (~85% of the maximum force at d = 3 µm). Maximum forces of ~50 pN with 50 mW at the sample (Fig. 2), might allow, for example, the transport of an organelle moved by 7 kinesin motors to be arrested (assuming additive forces), which is usually difficult with other kinds of artificial probes. Alternatively, in comparison to other intracellular targets, the same maximum forces can be exerted on PBs at lower laser powers, which may help minimize trap-induced photodamage [37].

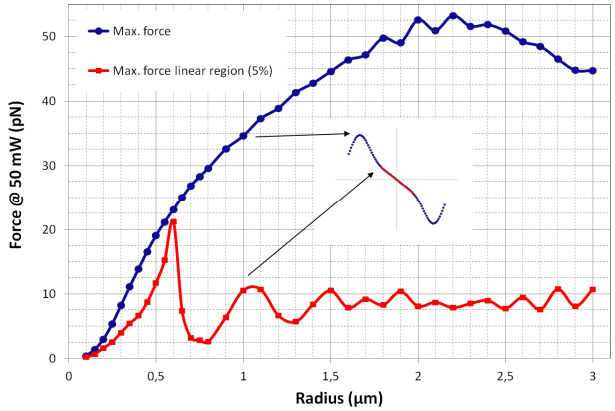

Fig. 2. T-matrix simulation [38] of the maximum force on a PB for different radii. (n_{PB} = 1.44). The maximum force within the linear region of the force curve is also shown.

3.2 Index of refraction

The dependence of the trap stiffness on the index mismatch between the sample and its surrounding environment (Δn) is, in general, a complicated non-linear function [39]. However, the destabilizing scattering force always increases faster than the gradient component with increasing Δn, eventually preventing stable trapping of high-index particles [14, 15]. Fortunately, in the range of values of biological interest, the maximum force exerted by an optical trap increases monotonically with the increasing index of refraction of the sample [40] and thus highly refractive organelles are suitable for the exertion of large forces inside cells.

Proteins show high refractive indices (n_p ~1.6) in pure form [41] so we expected PBs to share this feature. Indeed, the index of refraction of a protein solution, n_{ps}, is proportional to the concentration, c, according to a relation which stems directly from the Gladstone-Dale formula [41]:

$$n_{PS} = n_S + (\partial n / \partial c)\, c, \qquad (1)$$

where n_s is the refractive index of the solvent and (∂n/∂c) the refractive index increment. By consensus, the average refractive index increment is generally taken as 0.185 ml/g, although it is a quantity known to vary depending on the particular protein (estimated values range from 0.173 ml/g to 0.215 ml/g [42]). Although we have not yet explored the possibility, this variability may be used to control the refractive index of the resulting organelles through the expression of particularly appropriate protein sequences (oligomerization and then final density also depend on the particular Zera fusion).

#209469 - $15.00 USD Received 4 Apr 2014; revised 24 May 2014; accepted 25 May 2014; published 30 May 2014

Equation (1) is valid even for high concentrations of protein (exceeding 50%) [41] and is commonly used, for example, to determine the index of refraction of adsorbed protein layers [43]. It can easily be rewritten as a function of the densities [43] to give an estimation of the refractive index of PBs, n_{PB}:

$$n_{PB} = n_S + d_p\left(\left(d_{PB} - d_S\right)/\left(d_p - d_S\right)\right)\left(\partial n/\partial c\right), \tag{2}$$

where d_p, d_{PB}, and d_s are the densities of the pure protein, the PB and the solvent (assumed water) respectively. The density of PBs was found to be d_{PB} = 1.18-1.26 g/cm^3 by fractionation across density sucrose gradients of tobacco leaf homogenate extracts [30]. The density of a protein is a magnitude that loosely depends on its molecular weight, M (in kDa), according to [44]:

$$d_P = 1.410 + 0.145 \cdot \exp\left(M/13\right) g/cm^3, \tag{3}$$

Thus, for a typical Zera-derived fusion protein with a molecular weight of 40 kDa [45], we expect:

$$n_{PB} = 1.45 - 1.50, \tag{4}$$

a large value (Table 1). We can also calculate the index of refraction at the infrared wavelength that we use in our trapping experiments (λ = 1064 nm, the above calculation was made for green-yellow light). By inserting the corrected values [42]:

$$n_s = 1.324, \tag{5}$$

$$\left(\partial n/\partial c\right)_{1064} = \left(\partial n/\partial c\right)\left(0.940 + 20000/\lambda^2\right) = 0.177, \tag{6}$$

into Eq. (2), we finally have, for infrared light:

$$n_{PB}\left(1064\right) = 1.43 - 1.48. \tag{7}$$

We carried out two experiments to validate these estimations: a direct measurement of the index and an indirect estimation through the stiffness of a calibrated optical trap (Section 3.3). First, the refractive index of purified PBs was determined by means of the phase matching technique described in [41, 46, 47]. The technique is based on the observation, under phase contrast microscopy, of sample solutions with different refractive indices, n_{medium}. Particles with $n_{PB} < n_{medium}$ show up as dark bodies (negative contrast), whereas structures with $n_{PB} > n_{medium}$ are brighter than the surrounding medium (positive contrast).

As the refractive index of PBs, n_{PB}, was estimated to be around 1.5, we mixed diethylene glycol monobutyl ether (n_{butyl} = 1.4320) with 1-chloronaphthalene (n_{chloro} = 1.632) to produce the suspending media and fulfill the condition $n_{butyl} < n_{PB} < n_{chloro}$, as required. The refractive index of each resulting solution was measured with an Abbe refractometer (Edmund Optics 2WAJ).

#209469 - $15.00 USD Received 4 Apr 2014; revised 24 May 2014; accepted 25 May 2014; published 30 May 2014

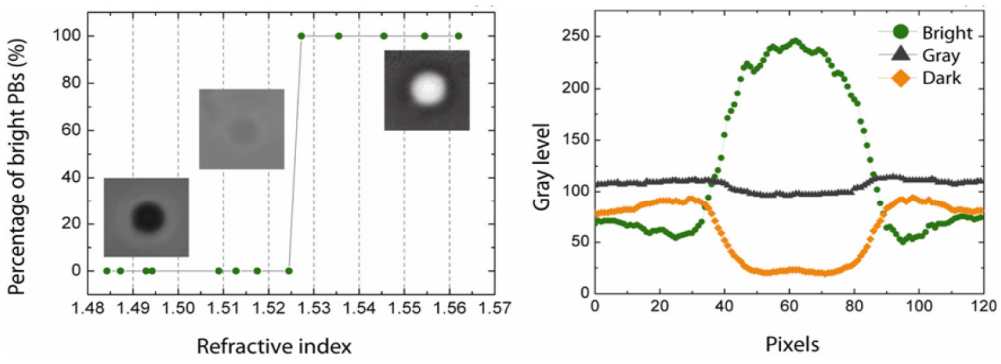

(a) (b)

Fig. 3. Determination of the index of refraction of PBs by means of immersion refractometry. (a) Percentage of bright PBs under phase contrast microscopy as a function of the refractive index of the suspension mixture and typical appearance of negative-contrast, almost index-matched, and positive-contrast PBs. (b) Brightness cross-section of the three PB images in (a).

Figure 3 shows the percentage of bright particles in a sample that contained multiple PBs, as a function of the refractive index of the suspension mixture. Typically, all PBs in the field of view appeared with the same contrast, changing from dark to bright simultaneously. Thus, the plot has the form of a step function in contrast to the error function distribution found in [47]. This is indicative of much higher homogeneity of our samples, (probably heightened due to purification by selective density centrifugation). The measured refractive index lies between $n_{PB} = 1.5245$ and $n_{PB} = 1.5270$, a value which is somewhat higher than that estimated by Eq. (4), but remarkably close considering the different factors that may affect the value of the refractive index increment in Eq. (1) (such as the solvent) [41].

3.3 Optical trap calibration and forces

The calibration of an optical trap *in vivo* is difficult since the cytoplasm of the cell shows viscoelastic properties. Thus, the Brownian spectrum of a trapped particle substantially differs from that observed *in vitro* using purely viscous buffers. Moreover, the elaborate calibration procedures required in a real cytoplasm [48] could be further complicated by the presence of ATP-dependent bio-active processes (such as the action of molecular motors) which are not included in the model. As a simpler alternative, and in order to obtain further experimental information on the optical forces that can be exerted on PBs, we measured the value of the stiffness, κ, for purified PBs of different sizes. PBs with sizes ranging from 0.54 to 1.48 μm (± 0.08 μm, see Methods), together with polystyrene beads (1.16 ± 0.04 μm), were suspended in a 70% solution of diethylene glycol monobutyl ether in water. The solution was prepared so that the measured refractive index (1.37) was similar to that of cytoplasm [49]. Also, a comparison of these results with simulation values of the stiffness provided us with an additional estimation of the index of refraction of the organelles at the infrared wavelength of our laser, in a similar approach to that reported elsewhere [39].

The particles were held in the optical trap and their Brownian motion tracked with back-focal-plane interferometry [50]. Using power spectrum analysis of the recorded data (Fig. 4), we determined the value of κ for 30 different PBs and several beads (Fig. 5). The Lorentzian fitting to the data was corrected to include aliasing, the detector transparency at infrared wavelengths and the frequency dependence of the friction coefficient [51]. The theoretical dependence of the trap stiffness on the particle size obtained with a T-matrix simulation [38] is shown for comparison. The linearly-polarized beam was focused through an $NA = 1.2$ water-immersion objective (overfilling of 1.4) to a spot with an estimated waist of ~0.4 μm [52]. The laser power at the sample (~50 ± 3 mW) was determined from the efficiency of our

#209469 - $15.00 USD Received 4 Apr 2014; revised 24 May 2014; accepted 25 May 2014; published 30 May 2014

back-focal-plane interferometer, as described in [52]. The theoretical and experimental curves match remarkably well assuming an index of refraction for PBs of n_{PB} = 1.44 (at λ = 1064 nm), in agreement with the estimation in Eq. (7).

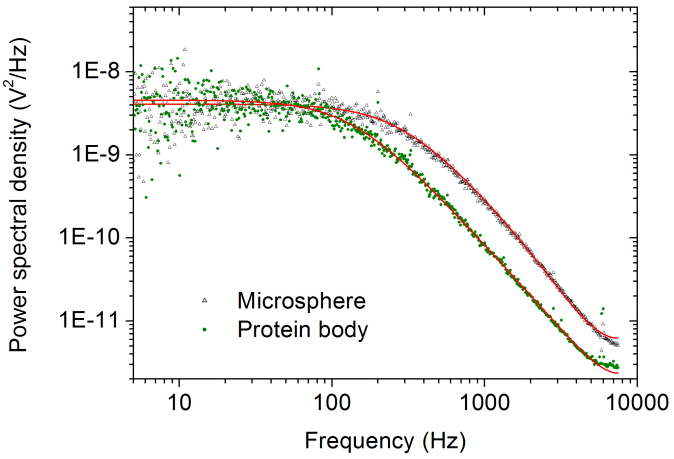

Fig. 4. Power spectra and Lorentzian fittings (red) of a trapped PB (green) and a latex microsphere of d = 1.16 μm (gray). Samples were suspended in a medium with a refractive index mimicking that of the cytosol (n_c = 1.37).

Also in accordance with the theory in Section 3.1, our results show a strong dependence of κ on particle size. As expected, the largest stiffness value is for objects with a diameter close to the laser wavelength in the medium (~800 nm). For this size, κ is up to twice the value of that for other diameters, so the target should be selected accordingly to maximize force production. We found PBs with sizes around this optimal value readily available in our purified samples and thus they should also be present inside the cell. When we compare the stiffness values with that of polystyrene beads, we observe that there is only a 50% difference between them. This difference is typically much larger for natural organelles (Table 1).

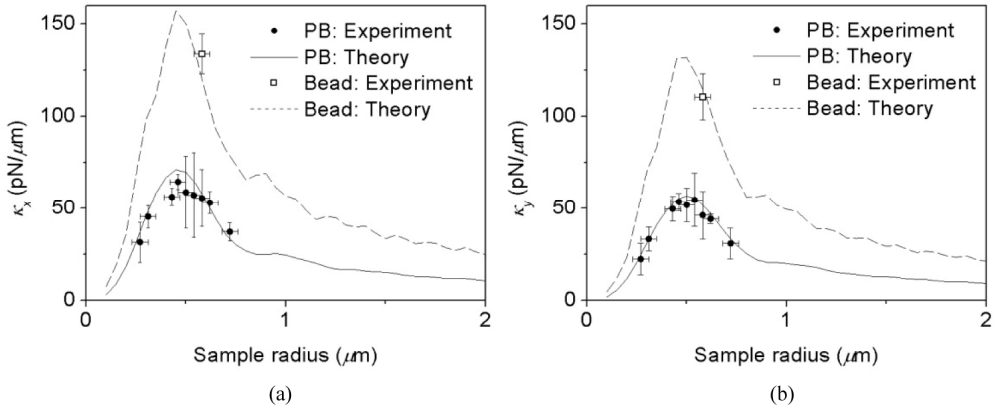

Fig. 5. Comparison between the measured (dots) and predicted (solid line) stiffness for different PB sizes in (a) x and (b) y directions. The theoretical curve for the polystyrene microspheres is also included (dashed line). Each point is the average of 2-3 different samples. Error bars represent standard deviations.

#209469 - $15.00 USD Received 4 Apr 2014; revised 24 May 2014; accepted 25 May 2014; published 30 May 2014

Table 1. Intracellular targets and characteristics of the resulting optical traps.

Organelle	Size (diameter, μm)	Index of refraction	Stiffness (pN/μm)	Fmax (pN)	Fmax linear (pN)
Mitochondria [53]	0.4 (0.2 - 0.6)	1.40	10	2	1
Lipid droplet [22]	0.4 (0.3 - 0.5)	1.46 - 1.53	24 - 35	4 - 5	2 - 3
Plant Golgi [54, 55]	0.5 (0.2 – 0.8)	1.40 - 1.50	17 - 55	3 - 9	1 - 4
Chloroplast [56]	5	1.40	5	28	5
Protein body [33]	1 (0.5 - 2)	1.45 - 1.53	83 - 140	21 - 38	13 - 25
Polystyrene bead	1	1.59	167	47	32

Power at sample = 50 mW, *NA* = 1.2, λ = 1064 nm. Fmax is the maximum trap force. Fmax linear is the maximum force within the linear region of the force curve (defined as the region where the linear approximation deviates by less than 5% from the true force curve).

4. Optical manipulation experiments

The extraction of lipid tubes from biological membranes requires considerably large forces *in vivo* (some tens of pN) [57, 58], so we carried out several experiments that involved the formation of membrane tethers via the application of force to PBs using an optical trap, as a proof of their application and advantageous properties. The experiments also allowed us to study the relationship between PBs and the organelle from which they are generated: the ER. The experiments were carried out in epidermal leaf cells of *Nicotiana benthamiana*, but the results and the potential of PBs is not necessarily limited to these cells, since PBs have been successfully produced in several mammalian cell lines [30] (also Fig. 1(a)).

In plants, microtubules play a modest role in comparison to the actin cytoskeleton, which supports vesicle trafficking through the action of myosin motors [59]. The movement of organelles such as the Golgi apparatus, which in plant cells is composed of a multiplicity of particles, is either powered directly by myosins or indirectly though the vigorous streaming of the cytoplasm. The ER is constituted of a network of tubules and cisternae, and changes in their shape are associated with the actomyosin system and Golgi bodies [6, 55, 60]. PBs are formed in the lumen of the ER [33]. They often cluster into large, entangled clumps that can easily be found in the perinuclear and cortical regions of the cell. We carried out experiments with PBs located in these two regions.

We started by trapping, with the laser tweezers, PBs that were connected to a cytoplasmic strand near the cell nucleus (N). By pulling with the trap, we could easily isolate one single PB from the rest. A tether of stretched membrane formed, which still covered the particle (Fig. 6). The contact point (white arrow) was located on a membranous fluorescent structure inside the cytoplasmic strand, which was quickly streaming from left to right. The tether was pulled downstream, but maintained its connection with the ER membrane under the increasing tension until it was at an angle of ~65° with respect to the perpendicular to the cytoplasmic strand. These observations are similar to those reported by Ashkin and Dziedzic in scallion cells, and provide information about the viscoelastic properties of the cytoplasm and the driving force of the cytoplasmic streaming [61].

#209469 - $15.00 USD Received 4 Apr 2014; revised 24 May 2014; accepted 25 May 2014; published 30 May 2014

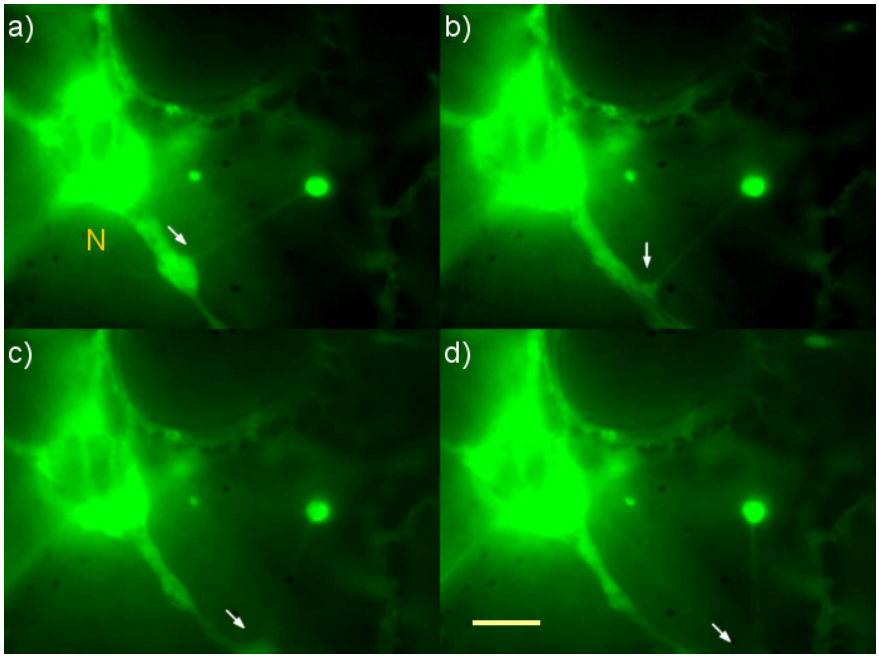

Fig. 6. A PB is trapped and pulled out near the nucleus (N). A membrane tether still connects the particle to a cytoplasmic strand that is streaming quickly. (a)-(c) The anchor site (arrow) moves together with the stream of the cytoplasm (from left to right). Scale bar: 10 µm.

We did not observe any noticeable deformation of the PBs subjected to the load. We specifically pushed two PBs against each other with optical traps (results not shown), but the two particles maintained their individual spherical shapes, behaving as rigid bodies. This agrees with the pure Lorentzian shape of the Brownian spectrum of trapped PBs (Fig. 4), and is relevant for the thermal calibration of optical traps and for the possible use of PBs in laser tracking microrheology, where the targets must be spherical and rigid to fulfill the underlying assumptions of the Stokes equation [62].

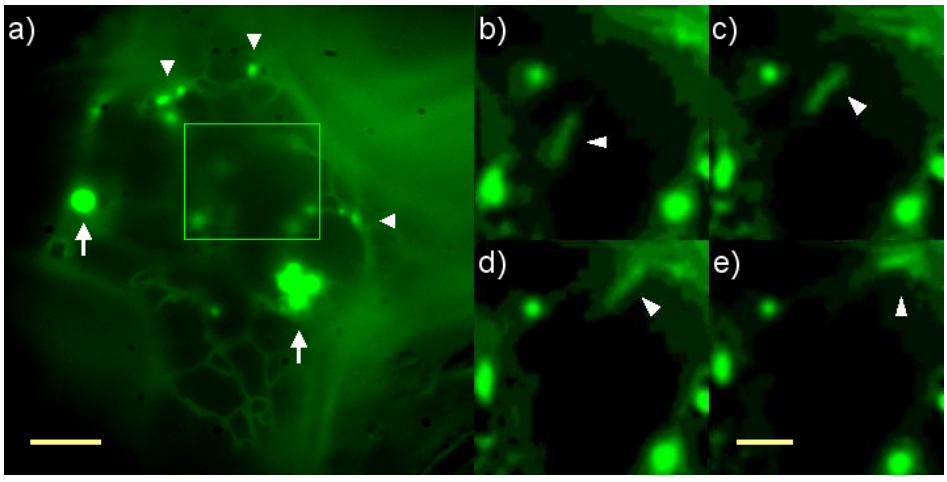

Fig. 7. (a) PBs (arrows) and Golgi bodies (arrowheads) are observed in a cortical region of the cell. The network organization of the ER is also visible (lower center). The box shows the region where images (b)-(e) were collected. (b)-(e) image sequence showing a Golgi body (arrowhead) moving through the cytoplasm, which is indicative of an intact cytoskeleton (time between frames = 0.5 s). Scale bar: 5 µm (a) and 2 µm (b-e).

#209469 - $15.00 USD Received 4 Apr 2014; revised 24 May 2014; accepted 25 May 2014; published 30 May 2014

We then proceeded to trap PBs connected to the cortical ER in the cell (Fig. 7). In plants, the movements that enable the continuous reorganization of the ER and Golgi bodies are actomyosin dependent. For example, the actin network forms a template over which the ER fits, in such a way that the shape of the organelle correlates with the distribution of the underlying actin filaments [55]. However, when the actin cytoskeleton is disrupted, the ER conserves its integrity and its characteristic polygonal shape, although it shows some morphological alterations [6, 55]. This relationship between the shape of the ER (and its function), the cytoskeleton and motile organelles such as Golgi bodies is not well understood.

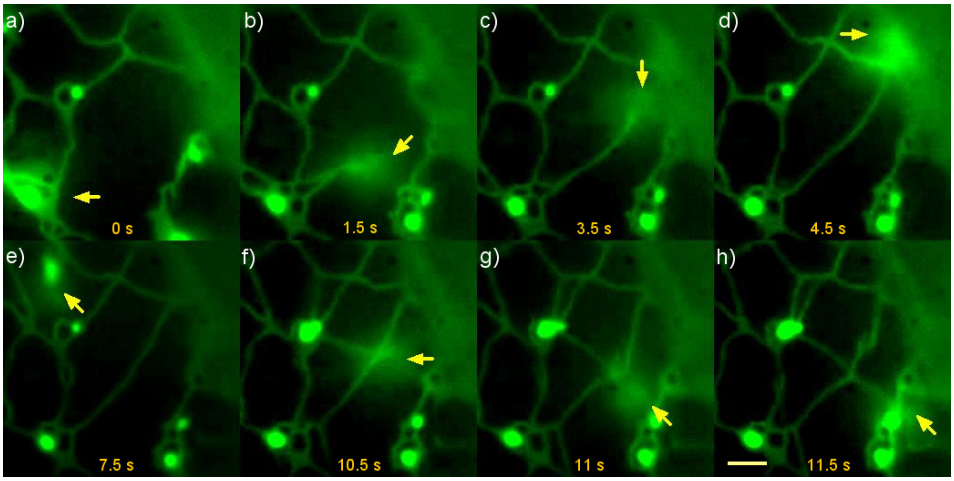

Fig. 8. A PB attached to an ER tubule is pulled through an empty region of the cytoplasm. The arrow indicates the approximate position of the optical trap. A circular movement of the laser spot creates a four-way junction of ER tubules, which intersect at right angles. Scale bar: 2 µm. See Media 1, first 14 seconds (scale bar in media: 2 µm).

Recently, optical trapping has been used to study some of these relationships in *Arabidopsis* epidermal leaf cells by pulling Golgi bodies physically connected to ER tubules [6]. Unfortunately, as the optical force that can be exerted on Golgi bodies is small (see Table 1), their motion first had to be abrogated by depolymerizing the F-actin with latrunculin B, prior to trapping. We carried out similar experiments but using PBs instead, which allowed us to maintain the cytoskeleton under physiological conditions (Fig. 8). A PB at rest is captured in the bottom left corner of Fig. 8(a) and pulled through the cytoplasm in circular motion. The PB remains connected to the ER through a thin membrane (tubule-like shape) that irreversibly extends following the movement. Contact with other structures in Figs. 8(d), 8(e) and 8(h) establishes anchor points for the newly created tubule. The vertical and horizontal sections of this ER tubule are made to cross at right angles in Fig. 8. At the contact point, the two sections of the tubule immediately fuse, creating a four-way junction.

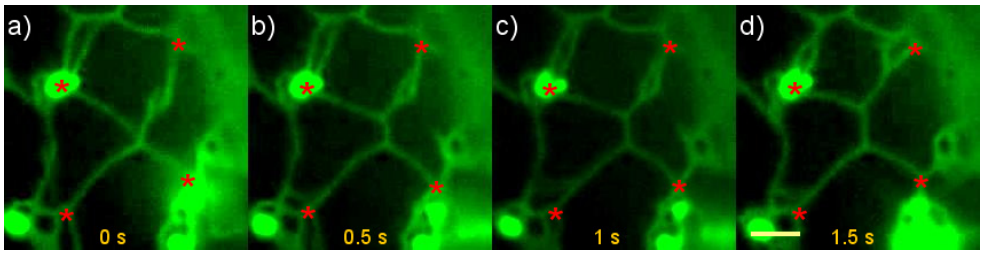

Fig. 9. The four-way junction artificially created with the optical trap quickly evolves into two three-way junctions. The vertical segment grows until all angles measure 120°, minimizing network length and thus free energy. The red stars mark the position of putative anchor points. Scale bar: 2 µm. See Media 1, between seconds 14 and 16.

#209469 - $15.00 USD Received 4 Apr 2014; revised 24 May 2014; accepted 25 May 2014; published 30 May 2014

However, this thin structure is short-lived and quickly gives rise to two three-way junctions (in less than one camera frame, 0.5 s, Fig. 9) connecting five straight segments. The central branch extends until all six angles measure 120°, thereby adopting a configuration that minimizes the total network length, L, and the surface free energy, F_t (which is proportional to L [57]).

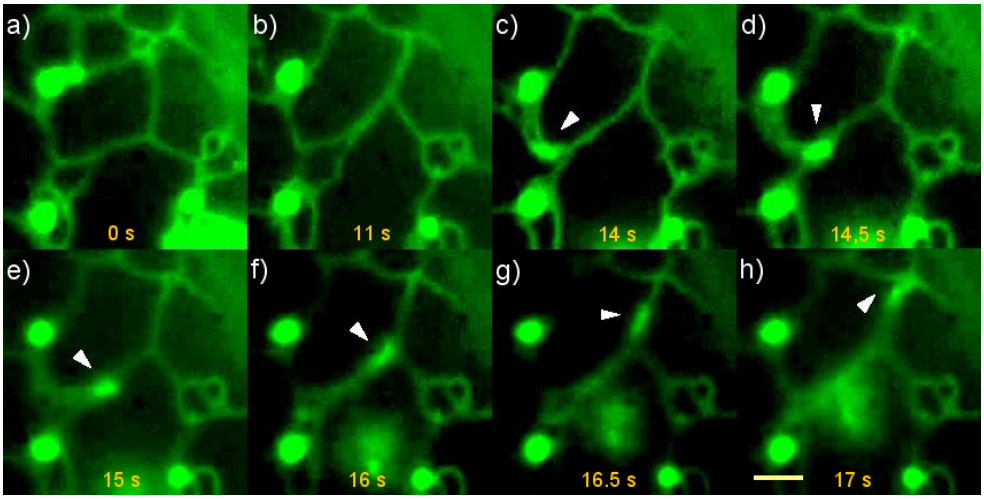

Fig. 10. The structure in Fig. 9 evolves into a single Y-junction and seems to align with an actin bundle as a moving Golgi (arrowhead) follows a trajectory coincident with that part of the network. Scale bar: 2 μm. See Media 1, after second 27.

Totally analogous configurations have been observed in synthetic lipid nanotube networks prepared *in vitro* by microelectroinjection [63]. The shape of the artificially induced section of the ER in Fig. 9 is clearly that of a free standing lipid tube network anchored at a few isolated points. However, this newly generated ER-like membrane tubule was not permanent and evolved for ~15 seconds, after which it spontaneously simplified into a single Y-junction (Fig. 10). Interestingly, part of this structure seems to align with an actin bundle, as a Golgi body can be seen to move along the same trajectory. This is reminiscent of observations made with a reconstituted system *in vitro* where elongated ER tubules pulled by myosin XI motors closely aligned to actin tracks [64].

In agreement with previous models [65], our results suggest that the overall shape of the cortical ER in plants is determined by a complex interplay between spontaneous energy minimization and interactions with the underlying actin cytoskeleton. Systematic repetition of optical trapping experiments with PBs as handles in similar intact cells may help clarify these questions.

5. Conclusions

Optical trapping is increasingly used to manipulate and probe structures or to measure forces in living cells once important insights have been obtained in controlled experiments *in vitro*. However, the transition into the cell is seldom straightforward, and techniques and tools that work well *in vitro* may prove inconvenient or inadequate *in vivo*. The use of phagocytized plastic microspheres as handles for optical traps is one such example. Trapping cell organelles is an alternative approach, but the physical properties of these objects, such as size, index of refraction, rigidity or homogeneity, are uncontrollable and often unknown, and so suboptimal for experiments.

To overcome these disadvantages, we artificially induced organelles and here we have discussed their use and applicability. PBs are spherical and rigid, have a near optimal size, a large and homogeneous index of refraction, and have no apparent side effects on the host

#209469 - $15.00 USD Received 4 Apr 2014; revised 24 May 2014; accepted 25 May 2014; published 30 May 2014

cells. These organelles allowed us to exert strong forces efficiently and, therefore, they could be advantageous substitutes for synthetic microspheres and other internal vesicles in optical trapping experiments.

The extension of these results to other cell types and the exploration of other useful properties of these organelles (motility, fluorescence emission, etc.) will require additional work.

6. Materials and methods

Optical trapping. We used a holographic optical tweezers system self-built around a commercial inverted microscope (Nikon Eclipse TE-2000E). In the setup, an Ytterbium-doped fiber laser beam (λ = 1064 nm, YLM-5-1064-LP, IPG Photonics) was collimated by a set of two lenses to overfill the phase-only spatial light modulator (SLM, X10468-03, Hamamatsu Photonics). After entering the microscope through the epifluorescence port, the beam was reflected upwards by an infrared dichroic mirror and focused at the sample plane by the objective lens. A second telescope was used to fill the entrance pupil of the objective lens, where we formed the SLM image [66]. We employed the following objective lenses for the optical manipulation of PBs: a Nikon Plan Apo 60x, 1.2 NA water-immersion lens, and a Nikon Plan Fluor 100x 1.3 NA phase contrast oil-immersion lens, which simultaneously enabled observation of the cells with a CCD camera (QImaging, QICAM). By means of an interactive user interface [67] we were able to dynamically create, move and remove traps as required. The microscopy system was complemented by an epi-fluorescence mercury fiber-illumination system (Intensiligh C-HGFI, Nikon). Simultaneous operation of fluorescence and laser tweezers was possible by stacking a second filter drum behind that carrying the laser dichroic filter. For the experiments with green (GFP) and red (dsRed) fluorescence proteins, this second drum contained a pair of filter cubes from Semrock (GFP-3035B-NTE-ZERO and CY3-4040B-NTE-ZERO). In all the experiments, tobacco leaf tissue was sandwiched between two coverslips and a silicone gasket (150 μm) was used as a spacer. The sample chamber was built so that water could flow through it in order to hydrate the sample, thereby ensuring the viability of the cells for extended periods. In vitro PB diameters were determined by means of image analysis software (ImageJ). To minimize ambiguities due to incorrect focusing, fiducial markers were selected in the intensity profile of a calibrated microsphere (d = 1.16 μm) which was coplanar with the PBs. These markers were in turn identified in the sample's profiles, which rendered the PB size in camera pixels. Finally, the known pixel size and objective magnification enabled us to relate camera units to real units (micrometers). We estimated the uncertainty of this procedure as ± 2 image pixels (equivalent to ± 0.08 μm at the sample).

Genetic constructs. Plant transformation. PB recovery. The plant transformation vector pCZera-DsRed, containing the sequence coding for the Zera-DsRed fusion, was obtained by replacing the ECFP (Enhanced Cyan Fluorescent Protein) sequence in pUC18ZeraECFP [30] with the DsRed reporter sequence and afterwards transferring the cassette containing this Zera-DsRed sequence to the binary vector pC2300 (http://www.cambia.org) under the control of the enhanced 35S cauliflower mosaic virus (CaMV) promoter.

Wild-type *Nicotiana benthamiana* plants are used for transient transformation. The plants were grown for 4-6 weeks in a greenhouse at 18°C-28°C, 55%-65% relative humidity and a photoperiod of 16 h. Individual *Agrobacterium tumefaciens* cultures (EHA 105 strain) transformed with binary plant vector pCZera-DsRed were mixed with an *Agrobacterium* culture carrying the HC-Pro silencing suppressor [68]. For transient transformation, the *Nicotiana benthamiana* plants were infiltrated with the transformed *Agrobacterium* culture by syringing into the abaxial side of upper three leaves [69].

Protein body isolation. 150 mg of agroinfiltrated tobacco leaf tissue was ground in a mortar at 0°C in 3.5 ml of an isotonic homogenization buffer (HB) containing Tris-HCl 10 mM pH 7.5, 0.25 M sucrose and protease inhibitors (plant protease inhibitors, Sigma, 1:250

#209469 - $15.00 USD Received 4 Apr 2014; revised 24 May 2014; accepted 25 May 2014; published 30 May 2014

dilution). The homogenate was filtered through two layers of Miracloth (22-24 μm, Calbiochem) to remove tissue debris and centrifuged at 100 x g for 5 minutes at 4°C. The resulting clarified homogenates were loaded onto multistep iodixanol (Optiprep, Sigma) density-based gradients (steps: 1.11, 1.17, 1.19, 1.21, 1.23 and 1.25 g/cm^3). For step gradient preparation, a working solution of 50% w/v (Y50) of iodixanol was prepared by mixing five volumes of Optiprep in one volume of 250 mM sucrose in HB buffer. Iodixanol steps were prepared by diluting the Y50 solution in HB buffer. Polyallomer centrifuge tubes of 12 ml were filled with 1.5 ml of each iodixanol step and 3 ml of clarified homogenate at the top of the tube. The gradients were centrifuged at 4°C for 2 hours at 24000 x g in a Beckman SW40 Ti rotor. Equivalent aliquots of supernatant, interphase fractions and pellet were analyzed by SDS-PAGE followed by protein staining in coomassie blue or immunoblot using specific antibodies. The PBs sedimented in the interphase of 1.21-1.23 g/cm^3 were collected by puncturing the tubes at the corresponding interphase. This interphase was diluted v:v with water, transferred to an Eppendorf tube and centrifuged for 10 minutes at 4°C. The PBs in the pellet were washed four times with 1 ml of water to be analyzed afterwards.

Mammalian cell transformation. CHO cells were grown in HAM F-12 (GIBCO) medium supplemented with 10% fetal calf serum (PAA), 2 mM L-glutamine (Sigma), 100 units/mL penicillin G (GIBCO) and 100 mg/mL streptomycin (GIBCO). Cells were grown in a humidified atmosphere (37°C / 5% CO_2). To transfect mammalian cells, the fusion protein coding sequence of Zera-ECFP from pUC18ZeraECFP [30] was introduced into the mammalian transfection vector pcDNA3.1(-) (Invitrogen) to produce the construct p3.1ZeraECFP.

Acknowledgments

This research was partly funded by the Spanish Ministry of Education and Science (FIS2010-16104, BFU-2009-07186 and BFU2012-33932) as well as by the regional authorities of Catalonia – ACC1Ó (VALTEC G614828324059231). C. L.-Q. acknowledges an APIF grant from the University of Barcelona and a A. F. an FI grant from the Generalitat de Catalunya (regional authorities of Catalonia).

#209469 - $15.00 USD Received 4 Apr 2014; revised 24 May 2014; accepted 25 May 2014; published 30 May 2014